Comparison Between Experimental and Numerical Results for a Research Hypersonic Aircraft

Pamela F. Richardson*
NASA Langley Research Center, Hampton, Virginia
Edward B. Parlette†
Vigyan Research Associates, Hampton, Virginia
and
Joseph H. Morrison,‡ George F. Switzer,‡ A. Douglas Dilley,‡ and W. Mark Eppard†
Analytical Services and Materials, Hampton, Virginia

Pressure and heat transfer computations obtained with a perfect gas, thin-layer Navier-Stokes code are compared with wind-tunnel data for a research hypersonic aircraft configuration at Mach numbers from 11-19. The effects of grid refinement/grid spacing away from the wall, nose bluntness, and turbulence are addressed. Results indicate that grid refinement in this study has little affect on the agreement between wind-tunnel data and computation for pressure, although it did have a significant affect on the agreement for heat transfer. Because of code capability constraints at the time the calculations were completed, the inflow boundary was assumed conical (sharp nose), whereas most of the wind tunnel tests were completed on a blunted configuration. Calculations show better agreement for heat transfer with wind-tunnel data for a sharp-nose model as compared to a blunted model. The use of the Baldwin-Lomax turbulence model improves the agreement between the computations and the turbulent wind-tunnel data; however, more sophisticated modeling is required to achieve better agreement with the wind-tunnel data. Overall, this initial comparison of computations with wind-tunnel data for a research hypersonic aircraft concept at hypersonic Mach numbers produced encouraging results.

Nomenclature

M_∞	= freestream Mach number
P/P_∞	= static pressure/freestream static pressure
Q_w	= heat transfer (Btu/ft^2-s)
Re_∞	= freestream Reynolds number/ft
T_∞	= freestream temperature, °R
y^+	= grid spacing parameter defined in Eq. (1)
Δy	= normal distance off the wall to the first grid point (in.)
α	= angle of attack (deg)
ν	= kinematic viscosity (ft^2/s)
ρ	= density (slugs/ft^3)
τ_w	= wall-shear stress (lb/ft^2)

Introduction

As the interest in hypersonic aircraft with air-breathing propulsion systems continues to increase, the need for design and analysis tools for these aircraft also continues to increase. Since program managers and engineers are attempting to accelerate the design of these vehicles, the classic method of aircraft design, that is, wind-tunnel testing, may not be viable for two reasons: facilities may not be available in the flow regimes required, and construction of those required facilities would not meet the time constraints of the design efforts. As a result of this existing situation, a tremendous dependence on computational fluid dynamics (CFD) to assist in the design process has emerged. Fortunately, advances in supercomputer speed and memory capacities, improvements in algorithms and numerical grid generation (both the geometry definition and flowfield grid), and the continuing efforts to expand CFD for complete aircraft configurations, have brought advanced CFD methodologies to the point that they can make significant contributions to the design process for these hypersonic vehicles.

Many of the advanced CFD codes that have been recently developed, however, have not been calibrated or validated with regard to their ability to correctly predict the flowfield and all performance parameters derivable from the flowfield. Generally, once a code is developed, a large effort is required to compare the code's predictions with other accepted codes and wind-tunnel and flight data. The CFD code used for the present calculations is currently undergoing extensive validation studies. In this paper, comparisons of wind-tunnel pressure and heat-transfer data with computations for a blended wing-body aircraft concept at Mach numbers between 11 and 19 are presented. Particle traces are shown in order to better understand features of the flowfield. A grid refinement study was conducted to determine if finer grids would improve heat transfer comparisons for high Reynolds number/turbulent flow conditions. The effects of nose bluntness on comparisons of the data are addressed. Finally, some comparisons between turbulent wind-tunnel data and computations using an algebraic turbulence model are shown to assess the difference between laminar and turbulent calculations.

Description of the Flowfield Code

The code used in this study was developed by Thomas et al.[1] The original code and its updated versions are identified as CFL3D. Although many researchers have been involved in the enhancements to this code, it still incorporates a set of upwind, finite-volume, shock-capturing algorithms that use either Roe's flux difference scheme[2] or van Leer's flux vector splitting technique.[3] The Roe's scheme is generally chosen over the van Leer scheme since the Roe scheme has less natural dissipation and, hence, more sharply defined shocks and more

Presented as Paper 89-0029 at the AIAA 27th Aerospace Sciences Meeting, Reno, NV, Jan. 8-12, 1989; received Feb. 25, 1989; revision received Sept. 16, 1989.

*Research Scientist, Computational Methods Branch, Fluid Mechanics Division. Member AIAA.
†Research Scientist.
‡Research Scientist. Member AIAA.

realistic boundary layers. Both upwind methods available in CFL3D have no adjustable smoothing parameters except for the choice of flux limiter. The minimum-modulus (min-mod) flux limiter (see Ref. 4) chosen for these calculations was the least dissipative available in the code.

The code originally solved the thin-layer Navier-Stokes equations for the external flow of a perfect gas using a Baldwin-Lomax turbulence model. Efforts are underway to enhance the features of the original code to include equilibrium air, internal flow analysis capability (with additional viscous terms), space marching algorithm (Parabolized Navier-Stokes), finite-rate chemistry, and a zonal-grid option. The current code employs a three-factor approximate factorization technique or a diagonalized scheme to iteratively update the solution in time. The solutions presented here were obtained on the entire flowfield grid in a time-dependent fashion. Solutions were converged to within a 0.001 change in the skin-friction drag coefficient over 300 iterations. With a grid of 200,000 points, a solution required approximately 15 million words of memory and 8–10 h of computer time on a machine on which the code operates at about 100 Mflops (million floating point operations per second).

At the time the present calculations were completed, the code was unable to calculate blunt body solutions, therefore, the present solutions were obtained by assuming conical inflow as the inflow boundary condition, i.e., the first two cross sections were scaled conically and the solution at the first cross section was set equal to the updated solution at the second cross section for each iteration. The initial conditions for the entire geometry were set to freestream conditions.

Wind-Tunnel Test Program

The wind-tunnel tests were completed in the Mach number range from 11 to 19 at angles of attack from 0 to 10 deg and at Reynolds number up to 10^7/ft. Both laminar and turbulent wind-tunnel data were obtained. The turbulent wind-tunnel data were obtained with both natural transition and forced transition (i.e., boundary-layer trips at the nose). The model, shown in Figs. 1 and 2, was instrumented with pressure and temperature gauges as well as pitot pressure rakes to determine the shock-layer and the boundary-layer thickness. Both blunt-nose and sharp-nose configurations were tested; however, most of the data were obtained for the blunt-nosed model. Even though the CFD code assumed a sharp nose, some comparisons are shown between blunt-nose and sharp-nose wind-tunnel data. Geometric features of the model are presented in inches; therefore, a fuselage station is designated as the distance in inches downstream of the nose along the streamwise axis of this model.

A preliminary analysis of the wind-tunnel data by the experimental program's team shows that the wind-tunnel data are generally accurate to within ±5%. This error analysis followed methods described by the National Bureau of Standards and represents the mean square root of the individual systematic errors. This error estimate is currently preliminary and will be finalized at a future date by the test facility. It was determined in a few cases that unsteadiness caused errors in some of the measurements to be as high as 26%.

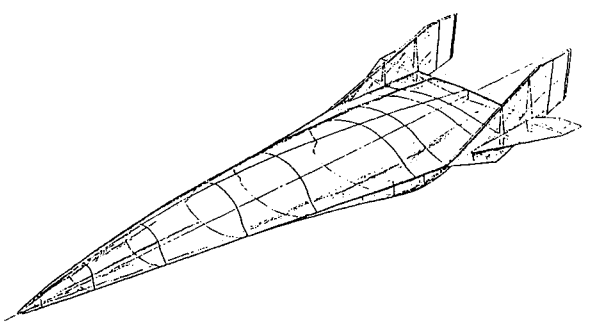

Fig. 1 Schematic of model geometry.

Flow Conditions

Seven wind tunnel runs were selected as test cases for comparison with CFL3D. They are listed in Table 1 (case 5 was run both laminar and turbulent). All seven cases were run on a $65 \times 65 \times 46$ grid (65×65 in the crossflow plane). The solutions were obtained downstream to just past fuselage station 26.75 (in.) since there was no instrumentation further back on the lower surface. More interest in lower surface data was initially the reason for this decision; however, as the program continued, some interest was generated in upper surface data. The upper surface has instrumentation past the 26.75-in. fuselage station. As a result, when the decision was made to run the higher Reynolds number solutions again with a finer grid, they were obtained on the entire 36-in. geometry. The high Reynolds number cases (Table 1, cases 5—laminar and turbulent—and 6) were recalculated on an $80 \times 130 \times 56$ (80 circum-

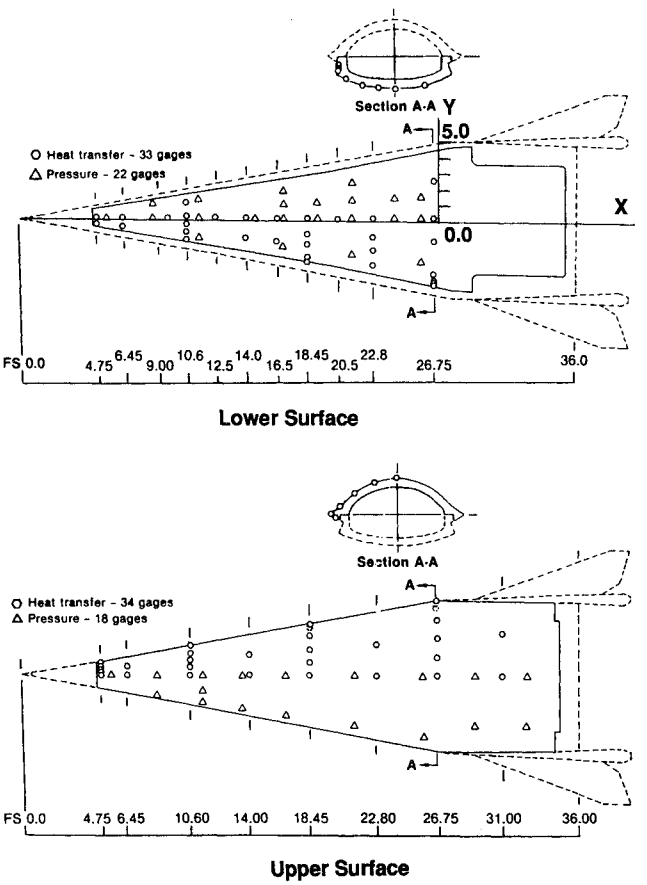

Fig. 2 Upper and lower surface model geometry with instrumentation locations; all dimensions (including fuselage stations, FS) in inches.

Table 1 Wind tunnel flow conditions used for calculations

Test case no.	Mach number	α	Reynolds number (/ft)	Freestream temperature, °R
1	12.4	0	5.8×10^5	166.7
2	12.4	6	5.8×10^5	166.7
3	16.6	0	1.1×10^5	81.4
4	19.2	0	3.6×10^5	88.3
5	11.35	0	9.9×10^6	109.4
6	12.55	0	2.7×10^6	129.7

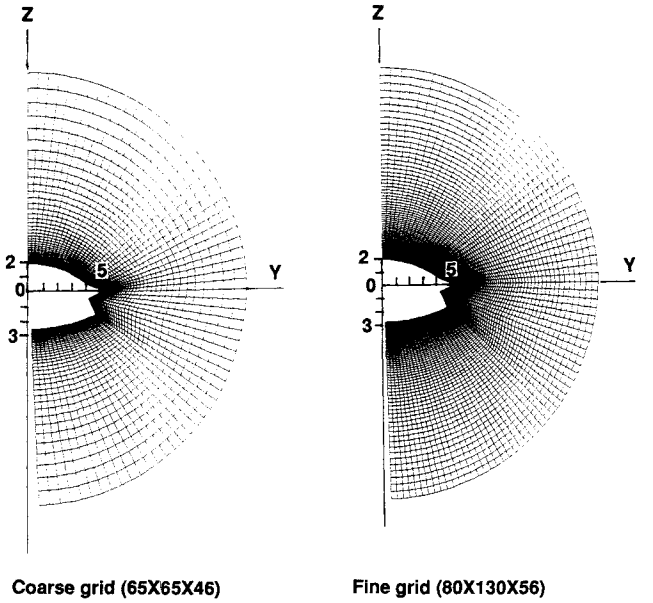

Fig. 3 Sample coarse and fine grids.

ferential and 130 radial) grid to determine whether grid refinement would improve the heat-transfer comparisons.

Geometry and Grids

The blended wing-body geometry used in this study is shown in Figs. 1 and 2. Although in Fig. 1 the model is shown with the wings and tails mounted, the computations were made on the configuration without wings and tails. The wind-tunnel data used for comparison with the computations were also obtained for the model without wings and tails. In Fig. 2 diagrams of the upper and lower surface of the model are shown along with pressure and heat transfer instrumentation locations. Dimensions shown on the drawing are in inches.

The grids were generated using transfinite interpolation (see Ref. 5). The coarser grid was stretched so that approximately 30 of the 65 radial points were intended to be in the boundary layer. As a result, resolution of the bow shock was not as sharp as it could have been had a finer grid been used in that region. The grid generation method can accept sharp changes in direction for the grid; therefore, sharp corners can be gridded. The grid at the surface was orthogonal, and the grid was nearly orthogonal near the surface. A sample of both the coarse and fine grids is shown in Fig. 3. Span and elevation dimensions shown in the figure are in inches. The fine grid was stretched so that approximately 60 of the 130 radial points were intended to be in the boundary layer. The grid spacing parameter y^+ was calculated on each cross section at the first point off the body and is defined as

$$y^+ = \Delta y \sqrt{\frac{\tau_w/\rho}{\nu}} \tag{1}$$

On any cross section, the maximum y^+ for the fine grid was 0.001, whereas the maximum y^+ for the coarse grid was 1. The minimum y^+ for the fine grid was 0.000001 and 0.001 for the coarse grid. The y^+ variations were seen in the grid axially, not circumferentially.

Results

The computational results presented in this paper are the second-order-accurate solutions on the $65 \times 65 \times 46$ grid with one solution shown on the fine grid ($80 \times 130 \times 56$). It was observed that the two different grids had little effect on the pressure results but significantly affected the heat-transfer results. Although it is generally accepted that a y^+ of 1 can give good results for heat transfer, it is shown in the following discussion that a grid with much smaller y^+ is required to match the wind-tunnel data more closely.

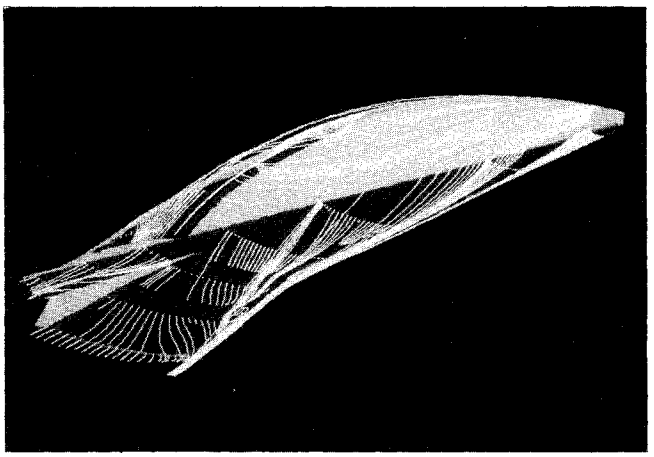

Fig. 4 Particle traces, Mach 19.2, 0-deg angle of attack, laminar, $Re = 3.0 \times 10^4$, grid $65 \times 65 \times 46$.

Calculations on both grids were completed to the same level of convergence. For the present study, the convergence criterion was chosen to be 0.001 in skin friction drag in 300 iterations. Because the finer grid provided the possibility of better boundary-layer and far-field (bow shock location) resolution, it was observed during the calculations that although the initial time steps for the fine grid were smaller, the subsequent time step could be ramped up more quickly than with the coarse grid. The fine grid had approximately three times the number of grid points as the coarse grid, which means that the computer time required to calculate one iteration on the fine grid was three times as great as on the coarse grid. However, since the time step increases were obtained more quickly on the fine grid, the total computer time to do one calculation—coarse or fine grid—was approximately the same. One complete solution took approximately 8–10 h of computer time on a vector-processing supercomputer running at 100 Mflops.

The following discussion will focus on data from the Mach 19.2 and Mach 11.35 cases. The Mach 19.2 case represents typical laminar results, whereas the Mach 11.35 case represents typical turbulent results. Both Mach number cases were calculated for 0-deg angle of attack.

Particle traces near the surface of the model are shown in Fig. 4 for Mach 19.2 and were obtained using the postprocessing color graphics code PLOT3D (see Ref. 6). General features of the flowfield can be seen from this figure. The most interesting feature of the flow near the surface is the buildup of flow along the lower surface centerline. This feature was also noted in the wind-tunnel data.

Pressure comparisons between the wind-tunnel data and computations are shown in Figs. 5 and 6 for the turbulent case at Mach 11.35 and in Figs. 7 and 8 for the laminar case at Mach 19.2. In these figures, the circle symbols represent available wind-tunnel data and the line represents the CFL3D solution on the coarse grid. Filled symbols represent lower surface wind-tunnel data. No fine-grid computational data are shown since analysis of the pressure computations showed little or no differences between coarse and fine grids. Figures 5 and 7 show the comparisons for the upper surface centerline and Figs. 6 and 8 for the lower surface centerline. Agreement between the wind-tunnel data and computations is generally within 10% and is considered good. There is some discrepancy on the lower surface for Mach 11.35 at the back of the model.

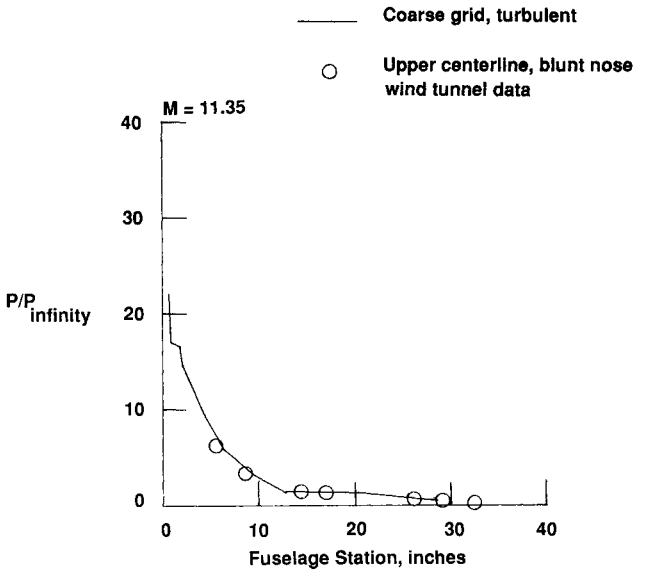

Fig. 5 Upper centerline pressure comparisons, Mach 11.35.

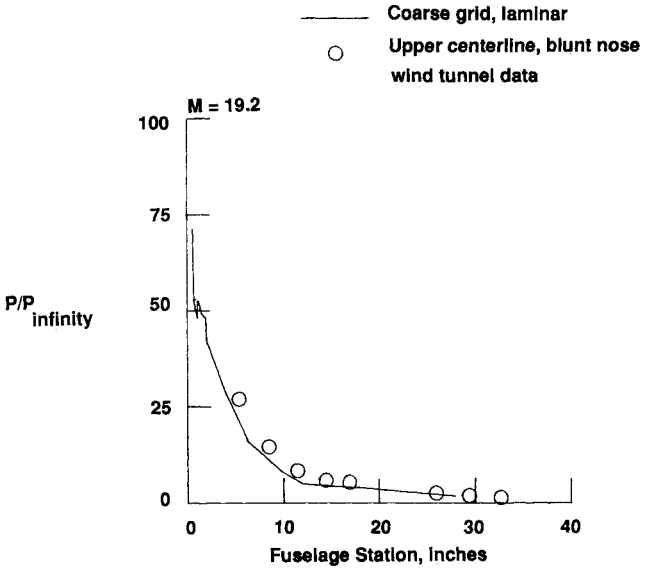

Fig. 7 Upper centerline pressure comparisons, Mach 19.2.

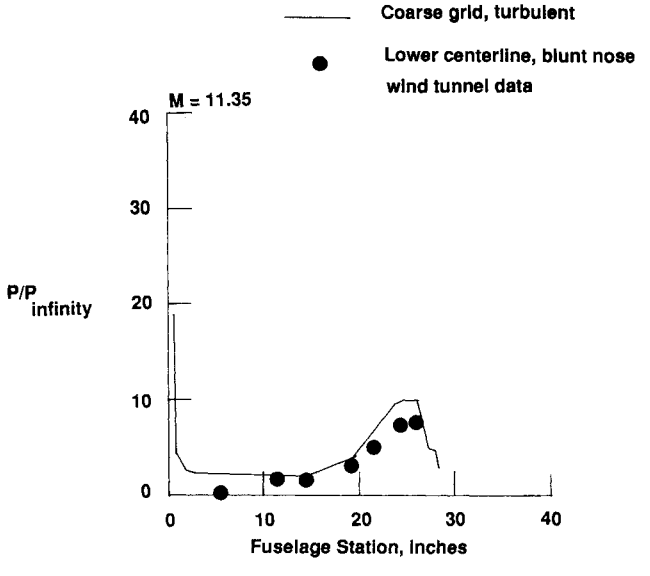

Fig. 6 Lower centerline pressure comparisons, Mach 11.35.

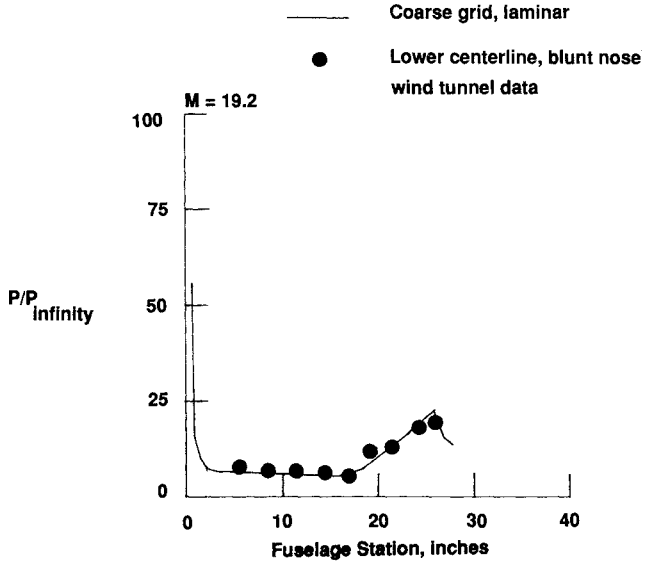

Fig. 8 Lower centerline pressure comparisons, Mach 19.2.

There is one wind-tunnel data point on the lower surface at Mach 11.35 (see Fig. 6) around fuselage station 5, which is practically zero. Although this is not stated by the experimentalists as being a bad data point, the authors of this paper suspect that it is.

Heat transfer comparisons between the wind-tunnel data and computations are shown in Figs. 9 and 10 for Mach 11.35 and in Figs. 11 and 12 for Mach 19.2. In Figs. 9 and 10, five sets of data are presented. Open symbols are upper surface wind-tunnel data and filled symbols are lower surface wind-tunnel data. Squares represent sharp-nose wind-tunnel data and circles represent blunt-nose wind-tunnel data. The solutions assumed a sharp nose since a blunt-nose assumption in the code was not available at the time of the calculations. The solid line on these plots represents the fine-grid, turbulent solution at Mach 11.35. The dashed line represents the fine-grid, laminar solution at Mach 11.35. Finally, the dashed-dotted line represents the coarse grid, turbulent solution at Mach 11.35. Figure 9 shows the upper centerline data. Note that the sharp-nose wind-tunnel data and fine-grid, laminar solution agree best on the front of the model. This is an indication of possible laminar flow on the upper surface of the model. Toward the back of the model, the sharp-nose wind-tunnel data agree better with the fine-grid, turbulent solution indicating a possible transition on the upper surface near the back of the model. Agreement is generally within 10% and is considered good. The difference between blunt and sharp wind tunnel data is not significant on the upper surface.

Figure 10 shows the lower surface centerline data. Near the nose, the fine-grid, laminar solution and sharp-nose wind-tunnel data show the best agreement, whereas further back on the model, the fine-grid, turbulent solution agrees best with the sharp-nose wind-tunnel data. On the lower surface, the effects of bluntness seem to be greater than on the upper surface, as differences between blunt and sharp wind tunnel data vary as much as 50%. It should be noted that transition may be occurring around fuselage stations 8–10 since the wind-tunnel data tend to agree better with the turbulent CFD solution past that fuselage station. This is an observation by the authors based on the comparisons shown. Upon completion of discus-

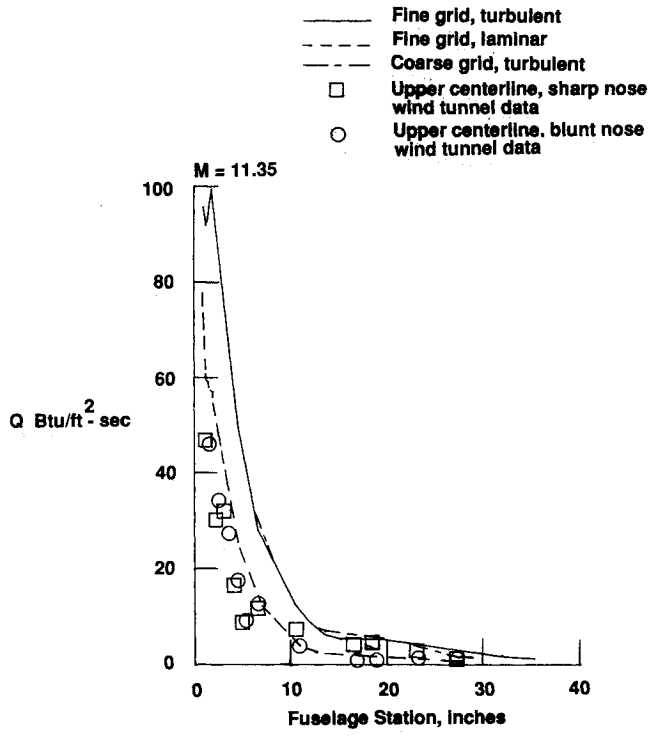

Fig. 9 Upper centerline heat-transfer comparisons, Mach 11.35.

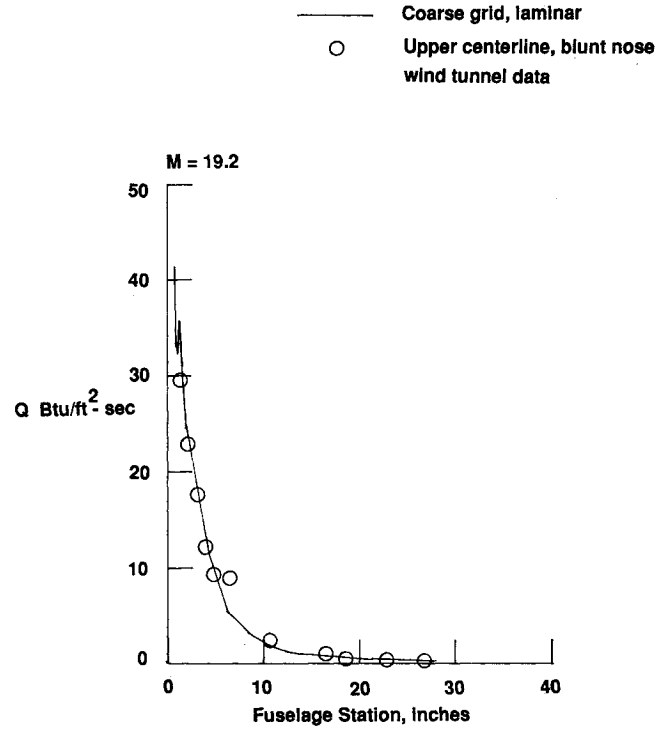

Fig. 11 Upper centerline heat-transfer comparisons, Mach 19.2.

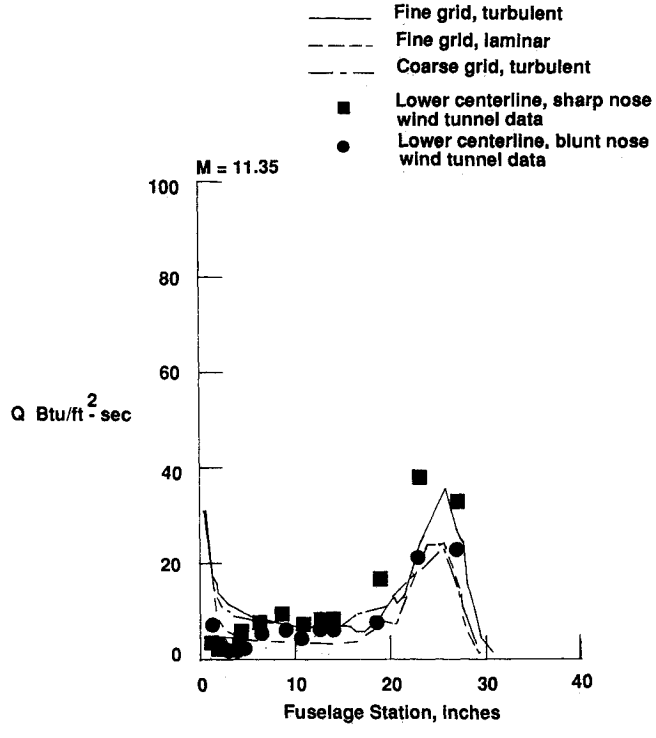

Fig. 10 Lower centerline heat-transfer comparisons, Mach 11.35.

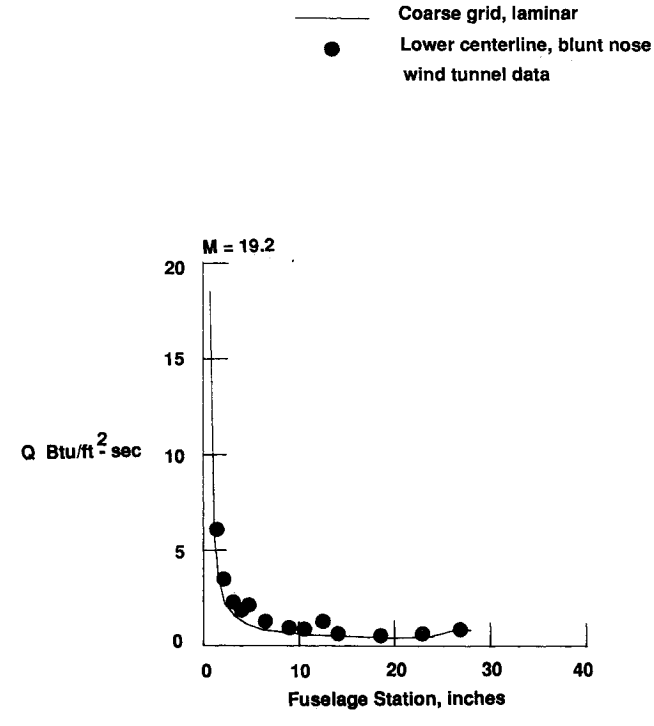

Fig. 12 Lower centerline heat-transfer comparisons, Mach 19.2.

sions with the experimental team, this transition location was confirmed for the wind-tunnel data. Since no transition criterion was assumed in the present computations, the calculations were completed assuming either fully laminar or fully turbulent flow. At the time of the calculations, this transition capability was not in the code. Subsequently, however, simple transition models have been installed in the code and are currently being tested. It appears from the comparisons shown here that advances both in transition and turbulence modeling are needed to improve agreement between experiment and computation.

Figures 11 and 12 show comparisons between the wind-tunnel data and the coarse-grid, laminar solution at Mach 19.2. Agreement is good everywhere. In general, the laminar solution at Mach 19.2 agrees better with the wind-tunnel data than the turbulent solution at Mach 11.35, thus reinforcing the

need for advances in transition and turbulence modeling to improve agreement for turbulent flows.

Conclusions

Computations have been completed on a research hypersonic aircraft concept using the perfect gas version of CFL3D. These solutions have been compared with available wind-tunnel data. The effects of nose bluntness and grid refinement have been explored. In the present study, nose bluntness affects are seen from this study to be more significant on the lower surface of the model than on the upper surface. The finer grid improves the agreement between computations and wind-tunnel heat-transfer data and has little effect on pressure comparisons. Computational time for solution remained about the same for both the coarse and fine grid. This is believed because the fine grid better captures the flow physics and is therefore able to resolve the flowfield in fewer iterations. The fine grid not only contains more grid points but also has significantly smaller (at least two orders of magnitude) spacing away from the wall. A simple turbulence model was used to improve the agreement between computations and turbulent wind-tunnel data over laminar calculations; however, further improvement in the turbulent computations is indicated. It is also necessary to incorporate advanced turbulence modeling and transition criteria in the code. This initial study showed encouraging results and indicated that more work is required for verification of CFL3D as a validated CFD code for hypersonic flows.

Acknowledgments

The authors wish to acknowledge the involvement and assistance of the McDonnell Aircraft Company and the Calspan Corporation for the wind-tunnel test program. This test program was completed as a portion of the Generic Option 2 Code Validation contract for the National Aerospace Plane Program (NASP). The McDonnell Aircraft Company designed, built, and tested the model in Calspan's 96-in. shock tunnel. Data reduction was the responsibility of both organizations, and the final report of the contract may be obtained from McDonnell Aircraft Company, St. Louis, Missouri.

References

[1]Thomas, J. L., Walters, R. W., Rudy, D. H., and Swanson, R. C., "Upwind Relaxation Algorithms for Euler/Navier-Stokes Equations," NASA CP-2397, April 1985, pp. 89-107.

[2]Roe, P. L., "Characteristic Based Schemes for the Euler Equations," *Annual Review of Fluid Mechanics*, Vol. 18, 1986, pp. 337-365.

[3]van Leer, B., "Flux-Vector Splitting for the Euler Equations," ICASE Rept. 82-30, Sept. 1982.

[4]Anderson, W. K., Thomas, J. L., and van Leer, B., "A Comparison of Finite Volume Flux Vector Splittings for the Euler Equations," AIAA Paper 85-0122, Jan. 1985.

[5]Eriksson, L. E., "Practical Three-Dimensional Mesh Generation Using Transfinite Intepolation," *SIAM Journal of Science and Statistical Computations*, Vol. 6, No. 3, 1985, pp. 712-741.

[6]Walakta, P. P., and Buning, P. G., "PLOT3D User's Manual," NASA TM 101067, March 1989.